Nanostructured superhydrophobic surfaces

H. M. SHANG, Y. WANG, K. TAKAHASHI, G. Z. CAO*
Department of Materials Science and Engineering, University of Washington, Seattle, WA 98105, USA
E-mail: gzcao@u.washington.edu

D. LI, Y. N. XIA
Department of Chemistry, University of Washington, Seattle, WA 98105, USA

Superhydrophobic surfaces play an important role in many applications, such as contamination prevention, biocompatibility, enhanced lubricity and durability of materials [1–9]. Hydrophobicity is measured by the contact angle of pure water on a clean solid surface. When the contact angle is greater than 150°, the surface is considered to be superhydrophobic. The water–solid contact angle varies with the surface energy and roughness of the solid surface. The surface energy of a solid is determined by the surface chemistry, which in turn depends on the chemical composition and atomic arrangements at or near the surface. Structure relaxation, surface restructuring, and composition segregation all can reduce the surface energy and, thus, result in an increase in contact angle. However, such a reduction in surface energy would result in a limited increase in contact angle, and is insufficient to make a surface superhydrophobic. Usually trifluoromethyl carbon ($-CF_3$) containing diblock polymers, surfactants, or coupling agents are self-assembled on the solid surface to form a monolayer [10]. Surfaces terminated with trifluoromethyl carbon ligands possesses highest electron–fluorine affinity and consequently the lowest surface energy. Contact angle decreases when the $-CF_3$ monolayer is less than close-packed, but even on the fully packed monolayers, contact angle on a smooth surface generally does not exceed 120°. A further increase in contact angle and hydrophobicity, will require an increase in surface roughness [11].

The idea is conceptually straightforward; increased roughness will result in an increase in true surface area and, thus, lead to an increased nominal surface energy. Accordingly, the contact angle varies as dictated by Young's equation. It has been demonstrated that the contact angle will increase with increased roughness of a hydrophobic surface, whereas the contact angle will decrease with increased roughness of a hydrophilic surface. This relationship was established by Wenzel and referred to as Wenzel's law [12, 13]. However, Young's equation and Wenzel's law can only be used if the water droplet has complete contact with the rough surface. In reality, the contact between water and a hydrophobic rough surface cannot reach 100% and some air bubbles will be trapped at the interface. Consequently, the Young's equation should be modified accordingly [14]:

$$\cos\theta_{\text{rough}} = \Phi_s(1 + \cos\theta_{\text{true}}) - 1 \qquad (1)$$

where Φ_s is the fraction of the solid surface in contact with water, θ_{rough} is the nominal contact angle of a rough surface, and θ_{true} is the contact angle with no trapped air bubbles. From this equation one can see that two interfaces are attributed to the contact between a droplet and a rough surface. One is the interface between the droplet and the solid surface, and the other is the interface between the droplet and trapped air bubbles. The more air trapped between the rough surface and the water, the larger the contact angle will be.

Significant research has been reported on the study and synthesis of superhydrophobic surfaces that combine self-assembled trifluoromethyl monolayers and introduce surface roughness. Various techniques have been developed for creating the desired surface roughness. Examples include selective etching of grain boundary phases [15], inclusion of nanoclusters [16], using highly porous films [3, 17], and plasma-enhanced chemical vapor deposition of films [18]. Superhydrophobic surfaces have also been synthesized by pyrolysis of metal phthalocyanines, resulting in the formation of highly porous carbon nanotube and nanofiber films [6, 19, 20].

In this communication, we report a study on superhydrophobic silica surfaces based on roughness created by assembling various nanostructure materials. The objective of the present work is to relate the surface structure with superhydrophobicity as indicated by static and dynamic contact angles. Four different surface structures were created (as shown schematically in Fig. 1): (1) a smooth surface achieved by dip-coating sol–gel films, (2) an assembly of uniformly sized spherical nanoparticles, (3) a uniformly sized nanorod array unidirectionally aligned perpendicular to surface and (4) an open mesh of nanofibers lying parallel on a substrate. All the surface structures are created on a silica base material, which is subsequently covered with a self-assembled monolayer of tridecafluoro-1,1,2,2-tetrahydrooctyldimethylchlorosilane (TFCS, $CF_3(CF_2)_5(CH_2)_2(CH_3)_2SiCl$).

*Author to whom all correspondence should be addressed.

0022–2461

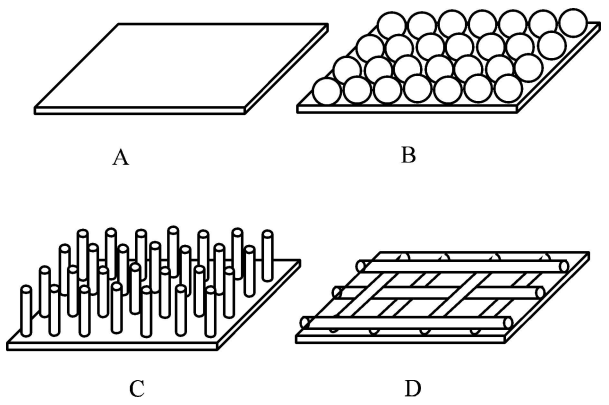

Figure 1 Schematically shows the four types of surface morphologies. A is smooth surface, B is assembly of uniformly sized spherical nanoparticles, C is uniformly sized nanorod array unidirectionally aligned perpendicular to surface, and D is open mesh of nanofibers lying parallel on substrate.

The smooth sol–gel coating (film A) was prepared from a sol (sol A) consisting of linear oligomers and formed a smooth surface upon removal of the solvent. This sol was prepared by admixing tetraethylorthosilicate (TEOS, $Si(OC_2H_5)_4$) and methacryloxypropyltrimethoxysilane (MPS, $H_2CC(CH_3)CO_2(CH_2)_3Si(OCH_3)_3$) and an HCl catalyst at a molar ratio of 95/5. First TEOS was partially hydrolyzed with a deficient amount of water and HCl in a solution at a molar ratio of TEOS/MPS/EtOH/H_2O/HCl of $0.95{:}0.05{:}3.8{:}1{:}1.2\times10^{-3}$ at 60 °C and stirred for 90 min. Then more water and HCl was added into the solution so that further hydrolysis and condensation reactions could proceed at 60 °C for another 30 min. The final sol had a molar ratio of TEOS/MPS/EtOH/H_2O/HCl of $0.95{:}0.05{:}3.8{:}5{:}4.8\times10^{-3}$. This method follows the same procedure as described by Chan *et al*. [21]. The film was made by dip-coating the sol on a glass substrate (micro slides, VWR Inc.), using a withdrawal speed of approximately 14 cm/min. The glass substrates were cleaned in excess ethanol by sonication for 10 min and rinsed with deionized water before coating. After coating, the sample was dried under ambient condition for 5 min and then heat-treated at 110 °C in air for 1 hr to remove the residual solvent.

The nanoparticle film (film B) was made from sol B—a mixture of TEOS and ethanol with NH_4OH (30% in water) as a catalyst. First 3 ml of NH_4OH was added into 50 ml of ethanol and stirred vigorously at 60 °C for 30 min, then 3 ml of TEOS was added dropwise. After 90 min of stirring the final sol B was obtained. These prepared sols consist of monosized spherical silica nanoparticles approximately 100 nm in diameter [22]. The film was made from the same procedure as film A, i.e., dip-coating and low-temperature sintering.

The nanorod array film (film C) was made from the same sol as that of film A, but the procedure used for making the film was a template-based capillary force approach. First, one drop of sol A was dropped on a cleaned glass substrate. Next a polycarbonate membrane consisting of pores 200 nm in diameter and 10 micron in length was placed on top of the sol. The sol was drawn into the pores by capillary force and solidified as the solvent evaporated. The filled membrane on the glass substrate was subsequently heated to 110 °C in air overnight and then sintered at 500 °C in air for 1 hr to remove the polycarbonate membrane. The resulting uniformly sized nanorod arrays adhered well to the substrate and were almost unidirectionally aligned perpendicular to the surface.

The nanofiber film (film D) was achieved through electrospinning. In a typical procedure, 1 ml of tetraethylorthosilicate (TEOS) was mixed with 1 ml of acetic acid, 7 ml of ethanol, 2 ml of water, and 0.42 g of poly(vinyl pyrrolidone) (PVP) (Aldrich, Mw = 1 300, 000). The solution was stirred for 5 hr in a capped bottle at room temperature before electrospinning. The electrospinning procedure was similar to the one previously reported by Dan Li [23, 24]. The PVP solution containing hydrolyzed TEOS was loaded into a plastic syringe equipped with a 23-gauge stainless steel needle. The needle was connected to a high-voltage power supply (ES30P-5W, Gamma High Voltage Research Inc., Ormand Beach, FL). The feed rate of the solution was set at 0.3 ml/hr using a syringe pump (KDS-200, Stoelting Co., Wood Dale, IL). The spin voltage was set at 7.5 kV. A piece of silicon wafer was placed 7.5 cm below the tip of the needle to collect the nanofibers. The collection time was 200 s. The as-spun nanofibers were left in air overnight to allow the hydrolysis of TEOS to complete. Finally, the PVP was selectively removed from these nanofibers by treating them in air at 500 °C for 1 hr. The resulting silica fibers are dense and approximately 100 nm in diameter.

The surface chemistry of all films was modified with a self-assembled monolayer (SAM). Prior to self-assembly, O_2 plasma etching was applied to remove organic components from the surface and to activate the surface sites through formation of hydroxyl groups after the material was subsequently submerged in water. The SAM was achieved by dipping all the films into a tridecafluoro-1,1,2,2-tetrahydrooctyldimethylchlorosilane (TFCS, $CF_3(CF_2)_5(CH_2)_2(CH_3)_2SiCl$) hexane solution with a concentration of 0.1 M. After 10 min the films were taken from the TFCS solution and washed with distilled water. The contact angle of distilled water was measured at room temperature (25 °C) directly after self-assembly with a manual contact angle goniometer (Model 100-00, Ramé-Hart, Inc.). The pictures of the contact angle were taken by a computerized microscope ($QX3^+$, Digital Blue). The surface morphologies were characterized by SEM (JSM 5200, JEOL) and AFM (Digital Nanoscope III, Veeco Metrology Group).

Fig. 2 shows the scanning electron microscopic (SEM) surface morphologies of four different films, which all closely mimic the schematic drawings presented in Fig. 1. For the sake of clarity and ease of comparison, all four pictures have the same magnification. Film A, made by dip-coating of a silica polymeric sol, is very smooth even at high resolution. Such sol–gel derived silica coatings are fairly dense and have pores inaccessible to nitrogen gas [21]. Film B is derived from the packing of uniformly sized spherical

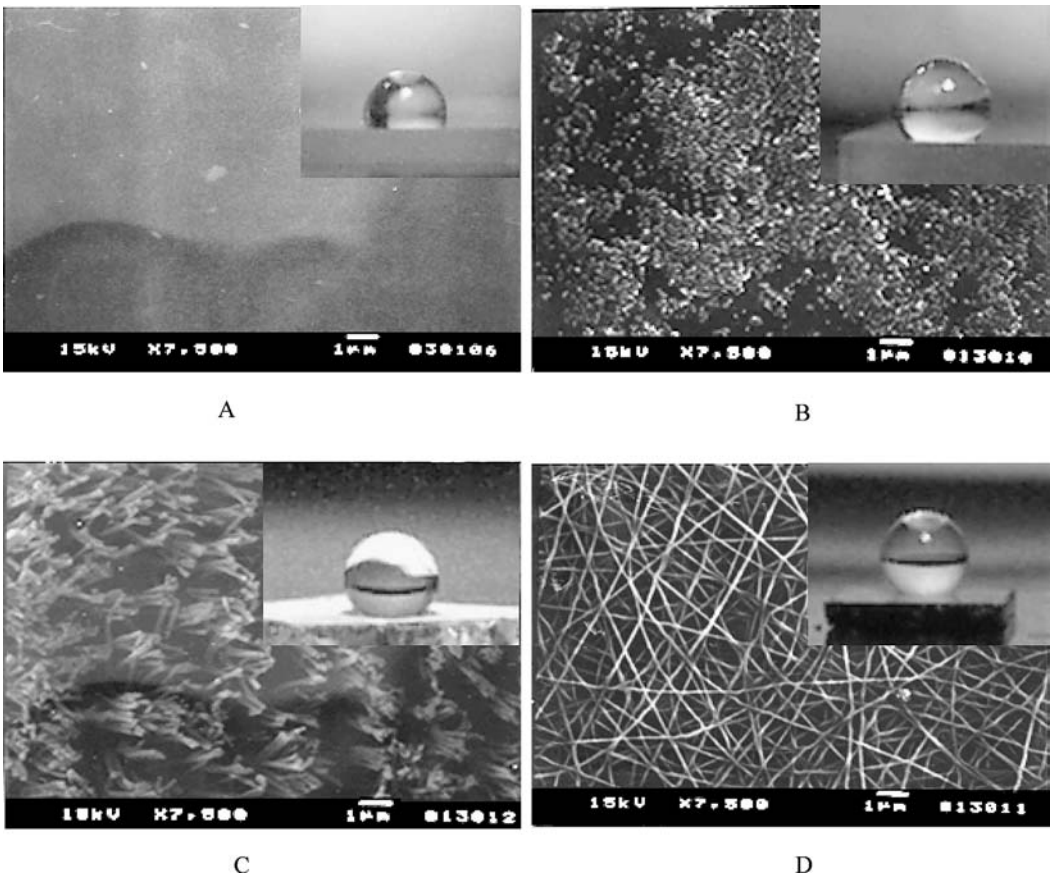

Figure 2 Contact angles and surface morphologies of four silica films with TFCS self-assembly monolayer. A, B, C, and D are smooth surface, nanoparticles surface, nanorods surface, nanofibers surface and their corresponding contact angles after self-assembly respectively.

silica nanoparticles. This method was first developed by Stober [25]. Although the dip-coating process was not optimized to ensure perfect coverage and an even distribution of the close-packed monolayer, the film is reasonably flat macroscopically with nanoparticles relatively evenly dispersed and covering most of the substrate surface. Film C consists of nanorod arrays aligned almost perpendicularly to the surface. All the nanorods have the same diameter ∼200 nm and are almost individually dispersed. The density of the nanorods is $\sim 10^9$ nanorods per square centimeter as estimated from the pore density of the membrane. The resulting gap between adjacent nanorods is significantly greater than that of the nanoparticle film. Film D is made by packing the nanofibers lying on the surface of the substrate. The largest gap between adjacent nanofibers exceeds 1 micron. Such a significant difference in surface morphology is better discussed in terms of surface roughness. The surface roughness of four films were denoted by root mean square (RMS) roughness which was determined directly from an AFM roughness analysis and summarized in Table I. The RMS of A is 0.5 nm, which is nearly a smooth surface, and B is 15 nm. Because the particles in film B are closed packed, the AFM tip can only measure the roughness of the packing surface, and can not go to the bottom of particles. This is the reason why the observed surface roughness is much smaller than the particle size which is ∼100 nm. As for films C and D, the roughness can not be measured accurately because the surface roughness of these two is far greater than that which can be determined by AFM. Not only are the gaps between adjacent nanorods or nanofibers in the micrometer range, but the differential height in these two films also exceeds 1 μm. However, AFM analyses do indicate unambiguously that the roughness of film C is smaller than that of film D, which corroborates very well with the SEM observation.

Fig. 2 also includes optical micrographs of water contact angles on four different nanostructured surfaces covered with a self-assembled TFCS monolayer (TFCS SAM) and clearly shows that the contact angle is strongly dependent on the surface morphology. Table I summarizes the contact angles measured before and after self-assembly of the TFCS monolayer. Prior to applying a TFCS SAM, all four films are hydrophilic with contact angles ranging from 10° to 17°. This observation can be explained qualitatively by Wenzel's law; increased surface roughness is expected to result in a decreased contact angle when the surface is

TABLE I Comparison of four surface structure morphologies and their corresponding contact angles

Films	θ_S (°)	$\theta_S^{\#}$ (°)	RMS (nm)	Φ_s
A	17	118	0.5	1
B	15	145	15	0.34
C	14	152	150–300	0.22
D	10	160	300–500	0.11

Note. θ_S: Contact angles before self-assembly; $\theta_S^{\#}$: Contact angles after oxygen plasma etching and self-assembly; Φ_s: fraction of the solid in contact with water (calculated based on the $\theta_S^{\#}$).

hydrophilic and the surface chemistry is identical. The difference in contact angle may also be attributed, at least in part, to the different surface chemistry. Since the initial silica precursors and other chemicals used in making sol–gel films (spherical nanoparticles, nanorod arrays, and nanofibers), were different, the chemistry of all four different surfaces would vary when no further thermal or chemical treatment was applied. However, the surface should be rather similar after oxygen plasma etching which removes all the organic components on the surface and etches some surface layers of the silica, subsequently resulting in the formation of hydroxyl groups on the surface when submerged into water. The contact angles after oxygen plasma etching are smaller than 2°, which is less than the detection limit.

All of the four films changed from hydrophilic to hydrophobic with static contact angles ranging from 118° to 160° when a TFCS-SAM was applied to the surface. The contact angles increased respectively in films A B, C, and finally D. Such increased contact angles are in accordance with the increased surface roughness. Hydrophobic surface, roughness will prevent water from contacting the solid surface completely by trapping air bubbles at the water–solid interface. From the static contact angle, the fraction of solid surface in complete contact with water, Φ_s, is calculated using Equation 1, and the results are also included in Table I. One can see that Φ_s decreases in the order of A > B > C > D films, which is in good qualitative agreement with the surface roughness as determined by AFM. An increased surface roughness results in a reduced contact area between solid and water due to an increase in air bubbles trapped at the interface, thus leading to increased static contact angles. This observation is in good agreement with the literature. For example, carbon nanotube and nanofiber films are reported to have achieved contact angles higher than 170° [6, 19, 20]. It should be noted that the present research is focused on the demonstration and comparison of the hydrophobic properties of various nanostructured surfaces. The optimization and formation of surface roughness and self-assembled monolayers are all expected to further improve the contact angles, but are beyond the scope of this communication.

A water droplet on a surface with a large static contact angle may remain pinned until the surface is tilted to a significant angle, and the difference between dynamic contact angles (advancing θ_A and receding θ_R contact angles) presents a clear indication of how stable the water droplet is on that solid surface. The contact angle hysteresis is more important in determining hydrophobicity than the maximum achievable static contact angle [1]. The following equation describes the force needed for a water droplet to start moving over a solid surface [26]:

$$F = \gamma_{LV}(\cos\theta_R - \cos\theta_A) \quad (2)$$

where γ_{LV} is the water surface tension. Table II presents the results from our further study of contact angles θ_A and θ_R for these four different hydrophobic films as well as the forces calculated from the dynamic contact angles. Advancing and receding contact angles were measured with the dispensing needle embedded in the sessile drop. Water was continuously supplied to the drop through the embedded needle until the sessile drop reached the maximum volume allowable for the liquid–solid interfacial area. At this point, any additional water would make the drop expand and increase the liquid–solid interfacial area. This contact angle is the advancing contact angle. As for the receding contact angle, water was removed from the drop until the liquid–solid interfacial area decreased. One can clearly see from the table that both advancing and receding angles increased in the same order as that of static contact angles, i.e., both advancing and receding contact angles increased with an increased surface roughness. However, the forces required to dislodge the water droplet varied in a slightly different pattern. The force required to move the water droplet on film A was more than twice of that of film C. The most noticeable difference is that film C has a smaller force than that of film D, though film D has a larger static, advancing, and receding contact angle than that of film C. This observation may be attributed to the different surface structures.

TABLE II Comparison of advancing and receding contact angles and force needed for a water droplet to start moving over a solid surface

Films	θ_A (°)	θ_R (°)	F (mN/m)
A	125	85	54.43
B	150	113	34.60
C	156	123	26.83
D	165	120	33.91

Note. θ_A: Advancing contact angles after self-assembly (SA); θ_R: Receding contact angles after SA.

The surface structures of the four films presented in this study can be divided into two groups: one surface is discontinuous in two dimensions and is formed by isolated building blocks (films B and C) without connection at the top of the surface, and the other possesses one or two dimensional continuity (film A with two dimensional continuity and film D with one dimensional continuity). In the cases of films B and C, when a water droplet rests on the surface, it is impossible to form a continuous contact line between liquid and solid. However in the case of film D, the surface consists of nanofibers lying parallel, and thus the liquid–solid contact is semi-continuous. This kind of continuous line can deviate from a circular shape as the droplet size increases to maximize contact with the solid and minimize the non-contact length. The result is the hysteresis effect of the surface which is an indicator of the larger difference between advancing and receding contact angles [27]. For a continuous contact line, when the volume of the drop is increased to advance the contact line, the drop will remain pinned until the contact angle is close to 180°, at which point the drop will jump from one metastable state to another. For a discontinuous contact line, the drop will not remain pinned (in a metastable state) and would move spontaneously on the surface by small incremental advances and recessions with no contact angle hysteresis [27]. In film C, because of discontinuous structure there is little or no

difference in energy between different states; thus there are no stable metastable states. As a result the force needed to let the droplet slide down is much smaller than that of film D.

In summary, four different kinds of silica-based surface morphologies have been synthesized by the assembly of various nanostructured building blocks and their respective hydrophobicity has been studied. Surfaces consisting of a nanofiber mesh demonstrated the highest static contact angle when covered with TFCS monolayers. However, surfaces consisting of nanorod arrays possesse the best dynamic hydrophobicity due to their discontinuous surface structure.

Acknowledgments

HMS acknowledges graduate fellowships from the Joint Institute for Nanoscience funded by the Pacific Northwest National Laboratory and the University of Washington. YW would like to acknowledge the Ford Company fellowship. The authors also want to thank Prof. John Berg, Prof. Alex Jen, Dr. Dong Qin, Dr. Richard Denial and Mr. Hin L. Yip for the permission and assistance in conducting the roughness and contact angle measurements as well as oxygen plasma etching.

References

1. W. CHEN, A. Y. FADEEV, M. C. HSIEH, D. ÖNER, J. YOUNGBLOOD and T. J. McCARTHY, *Lagmuir* **15** (1999) 3395.
2. A. NAKAJIMA, K. HASHIMOTO, T. WATANNABE, K. TAKAI, G. YAMAUCHI and A. FUJISHIMA, *ibid.* **16** (2000) 7044.
3. A. NAKAJIMA, A. FUJISHIMA, K. HASHIMOTO and T. WATANABE, *Adv. Mater.* **11** (1999) 1365.
4. T. ONDA, S. SHIBUICHI, N. SATOH and K. TSUJII, *Langmuir* **12** (1996) 2125.
5. K. TADANAGA, N. KATATA and T. MINAMI, *J. Am. Ceram. Soc.* **80** (1997) 1040.
6. H. J. LI, X. B. WANG, Y. L. SONG, Y. Q. LIU, Q. S. LI, L. JIANG and D. B. ZHU, *Angew. Chem. Int. Ed.* **40** (2001) 1743.
7. K. TADANAGA, J. MORINAGA, A. MATSUDA and T. MINAMI, *Chem. Mater.* **12** (2000) 590.
8. K. TADANAGA, N. KATATA and T. MINAMI, *J. Am. Ceram. Soc.* **80** (1997) 3213.
9. M. MIWA, A. NAKAJIMA, A. FUJISHIMA, K. HASHIMOTO and T. WATANABE, *Langmuir* **16** (2000) 5754.
10. TAKASHI NISHINO, MASASHI MEGURO, KATSUHIKO NAKAMAE, MOTONORI MATSUSHITA and YASUKIYO UEDA, *ibid.* **15** (1999) 4321.
11. S. H. WU, "Polymer Interface and Adhesion" (Marcel Dekker, New York, 1982).
12. R. N. WENZEL, *Ind. Eng. Chem.* **28** (1936) 988.
13. A. W. ADAMSON and A. P. GAST, "Physical Chemistry of Surface," 6th ed. (Wiley, New York, 1997).
14. J. BIEO, C. MARZOLIN and D. QUERE, *Europhys. Lett.* **47** (1999) 220.
15. K. OGAWA, M. SOGA, Y. TAKADA and I. NAKAYAMA, *Jpn. J. Appl. Phys.* **32** (1993) L614.
16. H. M. SHANG, Y. WANG, S. J. LIMMER, T. P. CHOU and G. Z. CAO, *Thin Solid Films* (in press).
17. H. Y. ERBIL, A. L. DEMIREL, Y. AVCI and O. MERT, *Science* **299** (2003) 1377.
18. A. HOZUMI and O. TAKAI, *Thin Solid Films* **303** (1997) 222.
19. H. J. LI, X. B. WANG, Y. L. SONG, Y. Q. LIU, Q. S. LI, L. JIANG and D. B. ZHU, *Angew. Chem.* **113** (2001) 1793.
20. L. FENG, S. LI, H. LI, J. ZHAI, Y. L. SONG, L. JIANG and D. B. ZHU, *Angew. Chem. Int. Ed.* **41** (2002) 1221.
21. C. M. CHAN, G. Z. CAO, H. FONG and M. SARIKAYA, *J. Mater. Res.* **15** (2000)148.
22. T. PHAM, J. B. JACKSON, N. J. HALAS and T. R. LEE, *Langmuir* **18** (2002) 4915.
23. D. LI and Y. XIA, *Nano Lett.* **3** (2003) 555.
24. D. LI, T. HERRICKS and Y. XIA, *Appl. Phys. Lett.* **83** (2003) 4586.
25. W. STOBER, *J. Colloid. Interf. Sci.* **26** (1968) 62.
26. E. WOLFRAM and R. FAUST, in "Wetting, Spreading and Adhesion" edited by J. F. Padday (Academic Press, London, 1978) p. 213.
27. R. E. JOHNSON JR. and R. H. DETTRE, *Adv. Chem. Ser.* **43** (1963) 112.

Received 6 October
and accepted 11 November 2004